Electrochemical Behavior of Gold Colloidal Alkyl Modified Silicon Surfaces

Guillaume Le Saux,[†] Simone Ciampi,[†] Katharina Gaus,[‡] and J. Justin Gooding*[,†]

School of Chemistry and Centre for Vascular Research, The University of New South Wales, Sydney, New South Wales 2052, Australia

ABSTRACT Herein, we report on the production of nanoelectrode arrays by attaching colloidal gold on silicon-bound mixed self-assembled monolayers of TFA-protected alkenylthiol (C_{11}-S-TFA) and undecylenic acid (acid). Effective modification of the surface, tethering of the nanoparticles, and the direct influence of the deprotected alkenylthiol (C_{11}—SH) /acid ratio on the number of adherent particles were demonstrated using X-ray photoelectron spectroscopy, electrochemistry, and atomic force microscopy. Cyclic voltammetry showed that the enhancement of electron transfer to the silicon surface by the presence of nanoparticles is influenced by the number of tethered nanoparticles.

KEYWORDS: hydrosilylation • mixed self-assembled monolayers • silicon surfaces • gold nanoparticles • blocking effect

INTRODUCTION

The development of nanoscale sensors is currently a research focus receiving a significant amount of attention (1). Important steps with regards to developing such sensors include synthesizing the nanoscale building blocks in the nanometer range (2, 3), having a method of modifying the surface chemistry properties, possessing appropriate techniques for patterning the modified layers (4), and using materials which are compatible with the bulk manufacture of devices. In this scope, silicon substrates have considerable potential because they are compatible with microelectronics (5, 6), they can be manufactured in massive parallel processes, as indicated by the electronics industry, and a range of patterning technologies exist. Furthermore, because silicon is being extensively used in the microelectronics industry, it is an easily accessible polymorph material with various bulk properties depending on the dopant type and its concentration (7). To form a sensing device, however, the silicon surfaces must be modified to enable à la carte control of how the sensing surface interacts with its environment. Perhaps the most controlled strategy of modifying any surface is via the formation of self-assembled monolayers (SAM) (8—10).

Originally, the most extensively studied SAMs deposited on silicon were alkoxy- and chlorosilane precursors (11—13). When the molecules are placed in a suitable solvent and an oxidized silicon surface is inserted, the trichlorosilyl head groups hydrolyze and chemisorb to the surface, forming Si—O—Si links to the surface (12, 14, 15). However, the presence of the insulating silicon dioxide layer (16, 17) may be a setback for the use of silicon as a substrate in electrochemical processes. Indeed, it was previously shown that electron transfer through a metal—insulator—semiconductor system was very sensitive to surface oxidation (18). Furthermore, although excellent voltammetry can be achieved for Si—O—C-bound SAMs on hydrogen-terminated silicon, the lack of stability of the monolayers highlighted the need for alternative synthetic strategies (19). In contrast, hydrosilylation chemistry, which requires the removal of that insulating oxide layer (8), will afford a chemically and electrically well passivated surface (17, 20—22) with a strong silicon—carbon bond and with a wide range of possible chemical functionalities (23—27). Furthermore, close to ideal redox behavior was recently achieved by functionalization of alkyne-terminated alkyl monolayers on highly doped silicon surfaces using "click" reactions to immobilize ferrocene derivatives (28, 29). The latter strategy represents a simple approach for the preparation of silicon-based electrodes where remarkable electrode stability can be achieved, opening a gateway for more use of semiconductors in electrochemically transduced sensing techniques.

The goal toward the construction of nanoscale electrochemical sensors on silicon has two main challenges.

(1) The first challenge is a stable and well-defined chemistry for the modification and passivation of the silicon electrodes such that they can operate in aqueous solutions. Typically, electrochemical experiments with silicon electrodes are performed in nonaqueous electrolytes (30). Although the hydride-terminated surface has a relative stability in air (31), the silicon must be passivated, as otherwise it will oxidize in aqueous solution as soon as anodic potentials are applied. As a consequence, recent studies using modified silicon electrodes in aqueous environments have only been able to probe the electrochemistry of species bound to the monolayer where the electrode surface was modified (17, 32).

(2) The second challenge is having a suitable end group for further connection of other electrodes or components (33).

* To whom correspondence should be addressed. E-mail: Justin.gooding@unsw.edu.au. Tel: +61-2-9385 5384. Fax: +61-2-9385 6141.
Received for review June 20, 2009 and accepted October 07, 2009
[†] School of Chemistry.
[‡] Centre for Vascular Research.
DOI: 10.1021/am900427w

Scheme 1. Schematic Showing the Different Steps in the Preparation of the Si(100) Surfaces[a]

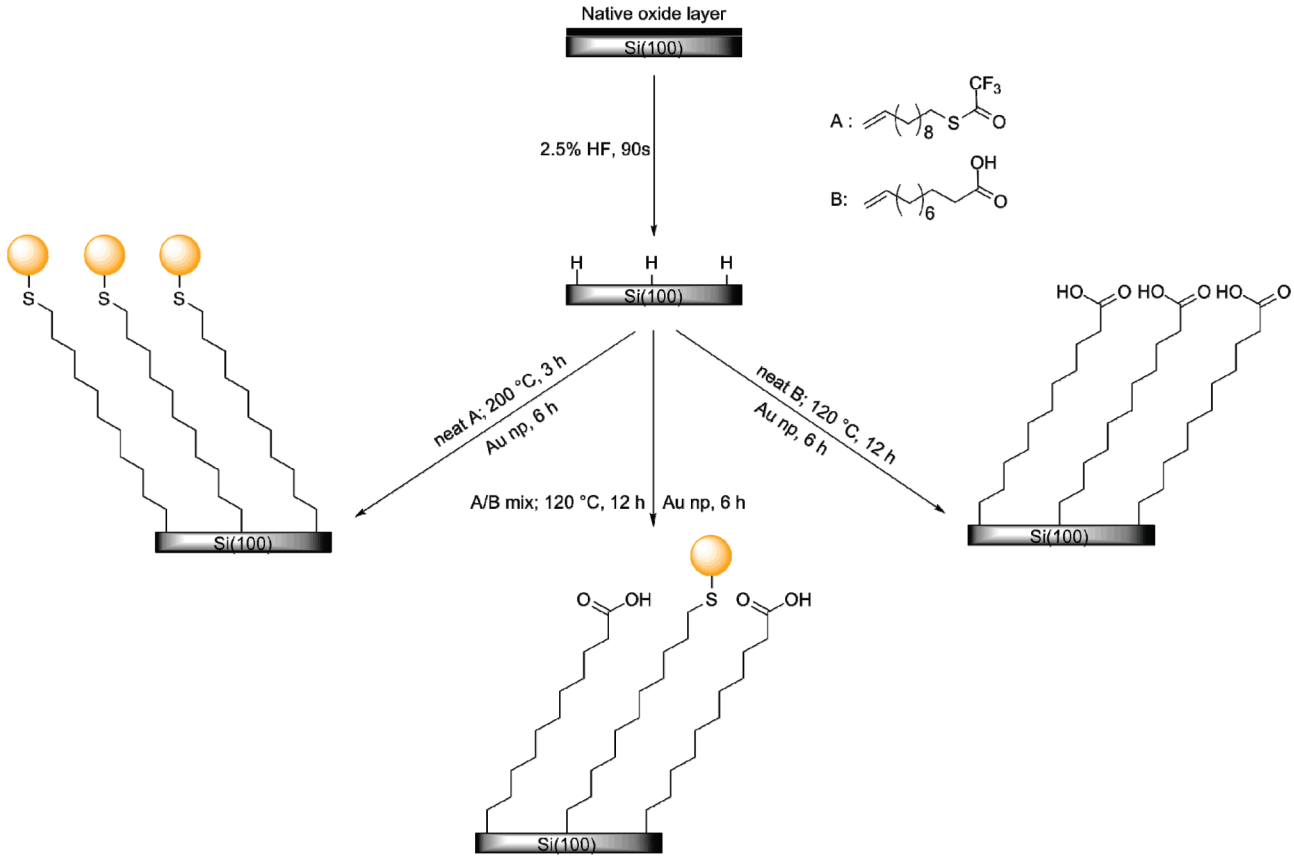

[a] Abbreviation: np = nanoparticles.

For both these challenges, monolayers derived from trifluoroacetyl (TFA)-protected alkenylthiol, recently demonstrated for the preparation of metal−insulator−semiconductor junctions (20, 34), hold some promise. Once assembled on a silicon surface, this molecule forms a good barrier to protect the silicon from appreciable oxidation. The removal of the TFA protecting group gives a thiol moiety that can allow metals to be covalently coupled to the distal end of the molecule. In previous work on molecular junctions, this thiol was used to connect to a mercury electrode. Equally well, however, nanoelectrode arrays could be produced by replacing the mercury droplet with metallic nanoparticles (35−37). The placement of nanoparticles on the distal end of the monolayer may allow solution species to be electrochemically interrogated by modified silicon electrodes (38, 39). The reason this seems possible is highlighted in a series of papers that have recently shown that electron transfer to electrodes that are otherwise passivated by a long-chain SAM can be greatly enhanced by adsorbing gold nanoparticles or carbon nanotubes onto the surface (36, 37, 40−48). It has recently been shown that with SAM-modified gold electrodes, onto which gold nanoparticles were adsorbed, the rate of electron transfer between the bulk gold electrode and a redox species in solution becomes independent of the thickness of the SAM (42, 47).

The purpose of this paper is to show that electrochemical communication between redox species in solution and a silicon electrode can be achieved using a passivating SAM further modified with gold nanoparticles. Nanoelectrode arrays were produced by forming silicon-bound mixed self-assembled monolayers of TFA-protected alkenylthiol and undecylenic acid (Scheme 1), analyzed by X-ray photoelectron spectroscopy and atomic force microscopy, and the influence of the assembly of nanoparticles on the response of the self-assembled monolayer to electroactive species in solution was demonstrated using cyclic voltammetry.

EXPERIMENTAL SECTION

Materials. Solvents were redistilled and, when required, dried over CaH_2 beforehand. Milli-Q water (>18 MΩ cm) was used for surface cleaning and reaction purposes. Semiconductor grade reagents were used for cleaning (30% H_2O_2, 98% H_2SO_4) and etching (2.5% aqueous HF solution). p-Type silicon wafers, with orientation (100) ±0.5°, 500 ± 25 μm thickness, and 0.007−0.009 Ω cm resistivity were purchased from Virginia Semiconductors, Inc. *S*-undec-10-enyl-2,2,2-trifluoroethanethiolate (C_{11}-S-TFA) was prepared in accordance to previous work (20) (see the Supporting Information).

Preparation of Au Nanoparticles. Colloidal gold particles with a size of 15−25 nm were prepared, according to the Turkevich et al. method (49), by adding 1.75 mL of 1% sodium citrate to 50 mL of boiling 0.01% $HAuCl_4 \cdot 3H_2O$, with vigorous stirring. Boiling was continued for 10 min, after which the solution was cooled with vigorous stirring (see the Supporting Information for an analysis of nanoparticles).

Preparation of the Monolayers. Modification of the Si(100) with the TFA-protected alkenylthiol was performed strictly according to literature methods (20, 34). Briefly, after thorough cleaning in piranha solution (3/1 v/v concentrated H_2SO_4/30%

H_2O_2), silicon wafers were etched in 2.5% hydrofluoric acid (HF) for 90 s to remove the native oxide layer. The freshly etched samples were then immersed in *S*-undec-10-enyl-2,2,2-trifluoroethanethiolate, which had previously been deoxygenated by a minimum of five freeze–pump–thaw cycles. The surfaces were left to react at 200 °C for 4 h. The wafers were then copiously rinsed with ethanol, ethyl acetate, and dichloromethane and blown dry under argon. A similar protocol was applied for surface modification with undecylenic acid and mixed alkenes with changes in the reaction conditions only. For example, surfaces modified with undecylenic acid were left to react at 120 °C for 12 h, and surfaces modified with mixed alkenes were left to react at 120 °C for 12 h.

Caution! Piranha solution reacts violently with organic materials and should therefore be handled with extreme care.

Caution! HF is an extremely corrosive acid; dilute HF solutions can cause delayed serious tissue damage and should therefore be handled with extreme care.

Preparation of Au-Modified Silicon Electrode. The derivatized surfaces were immersed in 10% aqueous ammonia for 5–10 min to remove the trifluoroacetyl group, followed by copious rinsing with Milli-Q water and ethanol, and blown dry under argon. The wafers were incubated a minimum of 6 h in the Au colloidal suspension, after which they were rinsed generously with Milli-Q water, ethanol, ethyl acetate, and then dichloromethane and dried under a stream of argon before sample analysis.

X-ray Photoelectron Spectroscopy. XPS experiments were performed using an EscaLab 220iXLwith a monochromated Al Kα source (1486.6 eV). Pressure in the analysis chamber was maintained below 10^{-9} Torr. Binding energies are referenced to the $Si2p_{1/2}$ signal (corrected at 99.9 eV). Spectral curve fitting was performed using the XPSPeak 4.1 software, with a convolution of Lorentzian and Gaussian profiles as described in previous works (20, 29) for the C1s, F1s, S2s, and Si2p regions. As for the Au4f region, a spectrum of bare gold was collected and a convolution of 35% Gaussian was found after fitting. A Shirley algorithm background subtraction was used for all regions.

Atomic Force Microscopy. Images were obtained using a Digital Instruments 3000 AF microscope in tapping mode. A minimum of three remote areas on the silicon surface were scanned for better appreciation of the modification with gold nanoparticles.

Electrochemical Measurements. Cyclic voltammetry was performed using a BAS 100B electrochemical analyzer and a three-electrode chamber (Inphaze Pty. Ltd.). The silicon surface was used as a working electrode, a gold wire as the counter electrode, and Ag/AgCl in 3 M NaCl as the reference electrode. The measurements were carried out in a 50 mM KCl solution containing 1 mM $K_3Fe(CN)_6$. Ohmic contact between the silicon samples and a copper plate was ensured by exposing the bulk of the silicon electrodes, using a diamond scribe, and rapidly applying a gallium indium eutectic onto the bare area. Silicon electrodes had a geometric area of 2 cm^2 with an area of 0.181 cm^2 exposed to the electrolyte solution using the Inphaze cell. Electrical impedance spectroscopy (EIS) data was acquired using a Solartron SI 1287 electrochemical analyzer with an SI 1260 Frequency Response Analyzer (Solartron Analytical, Hampshire, England).

RESULTS

Preparation of the Monolayers and Removal of the Trifluoroacetyl Protection. X-ray photoelectron spectroscopy (XPS) results shown in Figure 1 are in accordance with previous work (20, 34). For fluorine, the strong decrease in the large peak assigned to the CF_3 group at 689 eV confirms the near to complete deprotection of the monolayer, although traces of adsorbed fluorine also remain before and after deprotection, as shown by the second peak at a lower binding energy. For sulfur, since the S2p peak is obscured by the silicon loss peak at ~167 eV, narrow scans were performed around the S2s region (~228 eV). The S2s peak associated with a protected sulfhydryl group (229 eV) shifted to a lower binding energy, by ~1 eV, upon removal of the CF_3 protecting group. This is in good agreement with the binding energy of sulfur in a free sulfhydryl group. For carbon, the presence of C–C-linked carbons (285 eV), CF_3 (293 eV), carbonyl carbon (289 eV), and C–S-linked carbon (286.3 eV), in a ratio of 10.4:1.2:0.96:1 (expected ratio of 10:1:1:1), are consistent with previous work (20, 34). After deprotection, only C–C- and C–S-linked carbons remain, as well as some adventitious carbon species due to atmospheric contamination.

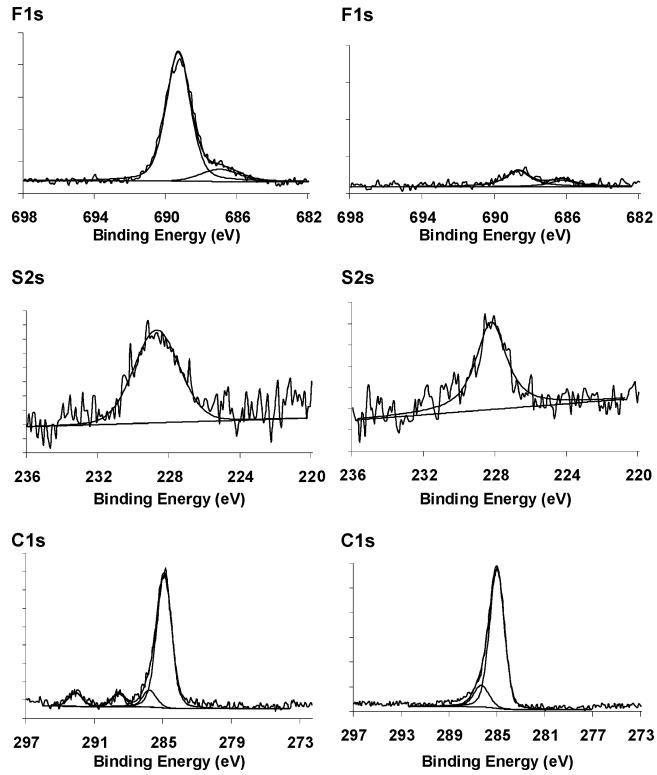

FIGURE 1. High-resolution XP spectra of F1s, S1s, and C1s regions of a TFA-protected alkanylthiol monolayer (left) and a deprotected alkenylthiol monolayer (right).

Preparation of the Au-Modified Silicon Electrode. Four types of SAM's were prepared, one 100% sulfhydryl terminated (C_{11}–SH), two mixed alkene SAMs with C_{11}-SH to acid ratios in solution of 1:10 and 1:100 (the ratio of 1:10 was chosen in order to have enough gold to ascertain the influence of the mixed SAM on the abundance of gold nanoparticles on the surface for XPS analysis), and one 100% undecylenic acid derived SAM. From the Au4f narrow scan of the C_{11}-SH surface after exposure to gold nanoparticles to give C_{11}-S-Au surfaces, the presence of gold is confirmed in the 100% sulfhydryl terminated surface (Figure 2a). Because of the high surface to volume ratio of the nanoparticles, it is possible to identify surface species adsorbed to the gold nanoparticles and differentiate them

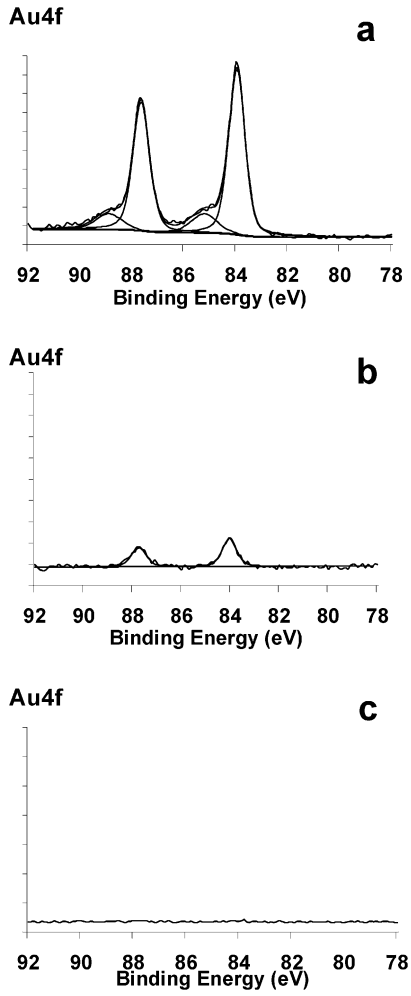

FIGURE 2. High-resolution XP spectra of the Au4f region of (a) C_{11}-SH, (b) 1:10 C_{11}-SH/acid, and (c) acid modified silicon, incubated in colloidal gold suspension.

from bulk gold in the Au4f narrow scan. This allows for the monitoring of any change in environment of the gold atoms at the surface of the nanoparticle. For example, it was possible to deconvolute a smaller peak in the gold narrow scan at higher binding energies (+0.5−1.0 eV), which is in good agreement with the case for Au−S-linked gold (50). The Au4f scan also allows the quantification of the Si:Au ratio. The atomic ratio of silicon to gold is 100:7.5. For the 1:10 mixed SAM (Figure 2b), the presence of gold is also confirmed and the atomic ratio is 100:0.8. Using these results, the relative amounts of gold on the 100% C_{11}-S-Au SAM to the 1:10 C_{11}-SH/acid mixed SAM was found to be 9.4:1. As shown in Figure 2c, the absence of gold for the undecylenic acid derived SAM confirms the effectiveness of the acid as a diluent to space the gold nanoparticle binding sites.

The XP spectrum in Figure 3 shows that some oxide is present on the surface, as seen by the hump in the 102−104 eV region. This is attributed to the fact that Si(100) surfaces are being employed. Most of the papers reporting a surface modification of silicon that shows little or no oxidation with alkenes do so on Si(111) (17, 22). Si(100) surfaces are significantly harder to passivate (17). The density of surface atoms plays a role in the ability to passivate the surface, as it is 7.83×10^{14} atoms/cm^2 for Si(111) and 6.78×10^{14} atoms/cm^2 for Si(100), resulting in a more densely packed SAM on Si(111) than on Si(100), thus making it harder for oxygen atoms to diffuse through and access the unreacted silicon atoms. Finally, it was reported that the oxidation rate of Si(111) is 0.4 times that of Si(100) (51).

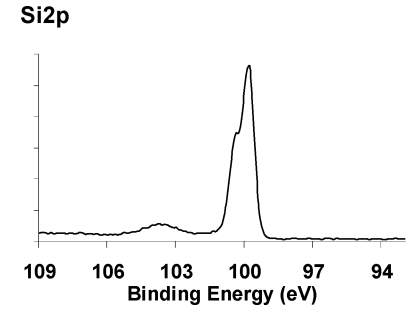

FIGURE 3. High-resolution XP spectrum of the Si2p region of C_{11}-S-TFA modified Si(100).

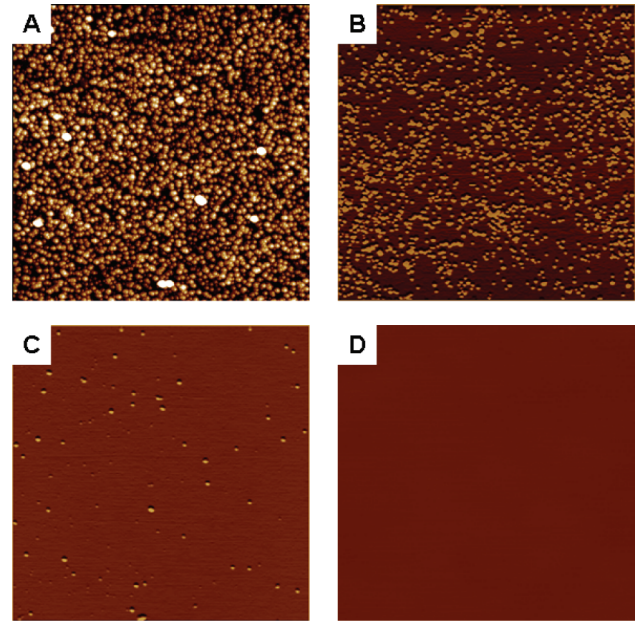

FIGURE 4. Analysis by AFM gold nanoparticle modified surfaces for the 100% C_{11}-SH SAM (A), 1:10 C_{11}-SH/acid SAM (B), 1:100 C_{11}-SH/acid SAM (C), 100% acid SAM (D). For all parts, the image size is 2 × 2 μm.

AFM images, as shown on Figure 4, confirm the presence of the nanoparticles on all surfaces except the undecylenic acid derived surface (Figure 4D). Although some clusters were noticed on the surface, the nanoparticles were randomly dispersed across the surface. Furthermore, the number of nanoparticles per unit area decreases for the 100% C_{11}-SH, 1:10 C_{11}-SH/acid and 1:100 C_{11}-SH/acid surfaces, respectively; values obtained are summarized in Table 1 (see the Supporting Information for quantification methods).

Here, the ratio of gold between the 100% C_{11}-SH SAM and the 1:10 mixed C_{11}-SH/acid SAM is 11.0:1; this value is close to that obtained by XPS, where it was found to be 9.4:1. For the 1:100 C_{11}-SH/acid SAM, this ratio falls to 107:1. Together, these results confirm the direct influence of the C_{11}-SH to acid ratio in solution on the number of tethered particles on the surface (see the Supporting Information for

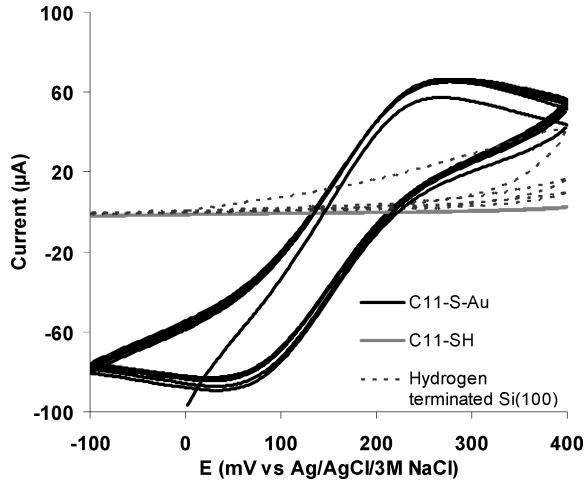

FIGURE 5. Cyclic voltammograms in 1 mM $[Fe(CN)_6]^{3+}$ for the C_{11}-S-Au modified surface (black curve), a C_{11}-SH SAM (gray curve), and a hydrogen-terminated Si(100) surface (black dotted curve). The first five cycles are shown.

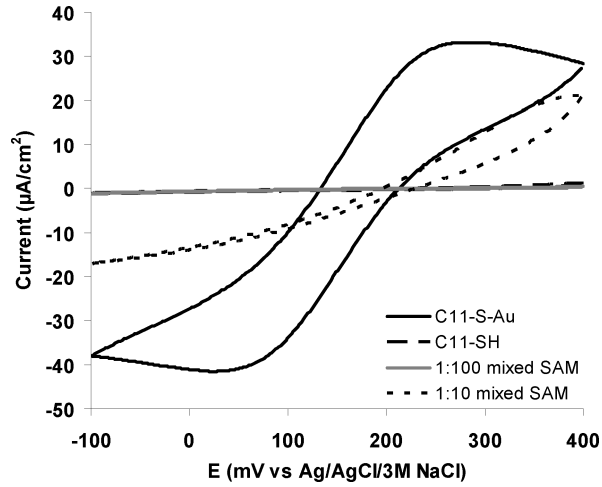

FIGURE 6. Cyclic voltammograms of 1 mM $[Fe(CN)_6]^{3-}$ in 50 mM KCl at 20 mV s^{-1} for the C_{11}-S-Au modified surface (black curve), the 1:10 mixed SAM (black dotted curve), the 1:100 mixed SAM (black dashed curve), and the C_{11}-SH SAM (gray curve).

Table 1. Number of Gold Nanoparticles per Unit Area and Ratio of Particles (i.e. Au on the 100% C_{11}-SH Surface/Au on the Surface in Question) for the Various Surface Types

	no. of particles/cm^2	ratio
100% C_{11}-SH	32.0×10^9	1
1:10 C_{11}-SH/acid	2.9×10^9	11.0
1:100 C_{11}-SH/acid	0.3×10^9	107

more detail on the XPS analysis of the 1:10 C11-S-TFA/acid mixed layer).

Electrochemistry of Silicon Surfaces. Figure 5 shows cyclic voltammograms (CVs) at a scan rate of 20 mV s^{-1} taken in an aqueous solution of 1 mM $K_3[Fe(CN)_6]$ with 50 mM KCl as background electrolyte of an C_{11}-S-Au modified surface (black curve), a C_{11}-SH SAM (gray curve), and a hydrogen-terminated Si(100) surface (black dotted curve). The hydrogen-terminated surface was obtained by dipping a Si(100) sample in 2.5% aqueous HF for 90 s prior to transfer to the electrochemical solution. The CVs shown are for the first five cycles that were performed on each type of surface. As can be seen for the C_{11}-SH SAM modified surface, the electrodes have very low capacitance and there is no evidence of a Faradaic process at all. The magnitude of the capacitance is unchanged with repeated scans. After attachment of nanoparticles the characteristic Faradaic oxidation and reduction of ferricyanide is observed, thus confirming that, as on gold surfaces, adsorbing gold nanoparticles onto an electrode passivated by a SAM facilitates electron transfer to the underlying electrode surface. Note, however, that the peak separation is large, almost 200 mV, indicating that the electron-transfer kinetics of the ferricyanide are much slower on these electrodes compared with the gold electrodes (42). For the hydrogen-terminated silicon, there were also no pronounced Faradaic peaks and the current was observed to decline with each cycle, where the electrode becomes more and more resistive. This decline in current is attributed to the oxidation of the silicon surface with each cycle and, hence, the formation of the insulating silicon oxide layer.

The influence of nanoparticle density on the electrochemistry is shown in Figure 6. The different mixed SAMs show drastic differences: the 1:10 mixed SAM exhibits some Faradaic process (black dotted curve), but with a reduction of the anodic peak and a near-disappearance of the cathodic peak in comparison with the 100% C_{11}-S-Au surface (black curve). This behavior is consistent with previous observations of surfaces with low coverage in nanoparticles (35). With the 1:100 mixed SAM (grey curve) the Faradaic process is almost completely suppressed and the CV is similar to that of the passivated surface (black dashed curve). This result shows that, at least on silicon surfaces, reasonably high surface coverage of nanoparticles is required for appreciable electrochemistry to be observed. It is, however, worth noting that there has been no evaluation of the impact of particle density on the ability of gold nanoparticles to facilitate electron transfer through passivating SAMs on gold electrodes. The previous detailed studies on gold electrodes by Fermin and co-workers and Shein et al. (42, 47) have had particle densities on the order of the 1:10 mixed SAM, and therefore, it is not clear whether the performance of these electrode−monolayer−nanoparticle systems is inferior on silicon compared with gold. What is clear, however, is that the rate of electron transfer is significantly slower on silicon than gold. The slower electron transfer kinetics is consistent with observations of electron transfer to ferrocene-modified SAMs on silicon and gold (32) and may have some impact on the electrochemical performance of the final devices.

EIS was used to assess the performance of the silicon electrodes (see the Supporting Information for details). Impedance spectra were run over a frequency range of 0.1−300 000 Hz at an applied dc potential of 0.21 V and an amplitude of 10 mV in 1 mM potassium ferricyanide. The resistance to charge transfer (R_{CT}) was determined by fitting

Table 2. Summary of Electrical Impedance Spectroscopy Data for SAM with Varying Nanoparticle Coverage

C11-SH:acid	coverage/cm^{-2}	R_{CT}/Ω	k_{et}/cm s^{-1}	k_{et}(np)/cm s^{-1}
1:1	9.09×10^{9}	6.74×10^{5}	2.18×10^{-6}	2.02×10^{-4}
1:10	1.88×10^{8}	5.70×10^{6}	2.58×10^{-7}	1.15×10^{-3}
1:20	1.16×10^{8}	1.16×10^{7}	1.27×10^{-7}	9.22×10^{-4}
1:100	1.71×10^{7}	1.39×10^{7}	1.06×10^{-7}	5.21×10^{-3}

the Nyquist plots to a conventional RC equivalent circuit, and the resulting rate of electron transfer was calculated using

$$k_{et} = RT/n^2F^2R_{CT}A[\mathrm{Fe(CN)_6}^{3-}]$$

where A is the area of the electrode. Results showed that the charge transfer resistance of the SAM-modified silicon electrodes decreases significantly with the presence of nanoparticles in comparison with the charge transfer resistance prior to nanoparticle immobilization of 2.0×10^7 Ω. Although the rates are much slower than those of gold electrodes, the observation of adsorption of gold nanoparticles drastically reducing charge transfer resistance is consistent with previous studies (36, 39, 42). Furthermore, the charge transfer resistance is sensitive to the nanoparticle coverage on the SAM (see Table 2). Using Fermin's modified theory of blocked electrodes, the rate of electron transfer per nanoparticle can be calculated using

$$k_{et}(\mathrm{np}) = RT/n^2F^2\Gamma\pi r^2R_{CT}Ac_{\infty}$$

where Γ is the particle coverage and r is the particle radius. The rate constant per nanoparticle was found to be in the range of 10^{-3}–10^{-4} cm s^{-1}, which is significantly slower than the values observed for ferricyanide with the analogous system on a gold substrate (47) and does not appear to vary with the particle density on the surface. The latter observation indicates these modified electrodes are acting as nanoelectrode arrays. On gold electrodes modified with SAMs and gold nanoparticles, the rate of electron transfer per particle was found to be similar to that observed for bulk polycrystalline gold electrodes (47). Hence, the slower rate constant here on silicon appears to reflect the difference in the underlying electrode material with a slower rate of electron transfer to silicon electrodes compared with gold (32).

CONCLUSION

In the present paper, robust alkyl -modified Si(100) with tethered gold nanoparticles were produced and characterized. XPS data showed that the nanoparticles were covalently bound to the surface and that they were inert to the carboxyl-terminated moieties. This allowed for the preparation of mixed trifluoroacetyl/10-carboxydecyl SAMs with variable nanoparticle coverage, as confirmed by AFM and XPS, albeit the presence of surface oxidation. Stable electrochemical measurements were obtained, and a direct influence of the nanoparticle coverage on the redox behavior of the surfaces was observed. The drastic drop in current density between the 1:10 and 1:100 C_{11}-SH/acid surfaces is a strong indication that a fairly high number of particles are needed for good signal transduction. This is a further indication that silicon is a material of choice for electrochemistry, as it can be easily modified to give substrates with high surface areas in the case of porous silicon for example (54).

The system used in this work is simple yet very promising for sensing applications. Indeed, a wide range of cysteine-labeled proteins, enzymes, and redox-active molecules is available and could be attached to the gold nanoparticles, making the surface target sensitive. Similarly, we have shown that the density of gold nanoparticles (nanoelectrodes) on the silicon surface can be tuned by altering the ratio of the two components in solution from which a mixed SAM is formed.

Supporting Information Available: Text and figures giving synthetic methods, an AFM analysis of the gold nanoparticles, the distribution of the nanoparticles on the different surfaces as well as an XPS analysis of the 1:10 C_{11}-S-TFA/acid mixed layer, and EIS data. This material is available free of charge via the Internet at http://pubs.acs.org.

REFERENCES AND NOTES

(1) Cai, D.; Chiles, T.; Kempa, K.; Naughton, M.; Ren, Z.; Trilochan, P. (The Trustees of Boston College). World Patent Application, 2008.
(2) Lehn, J. M. *Angew. Chem.* **1990**, *102*, 1347–1362.
(3) Wagner, R. W.; Lindsey, J. S.; Seth, J.; Palaniappan, V.; Bocian, D. F. *J. Am. Chem. Soc.* **1996**, *118*, 3996–3997.
(4) Loo, Y.-L.; Lang, D. V.; Rogers, J. A.; Hsu, J. W. P. *Nano Lett.* **2003**, *3*, 913–917.
(5) Ashkenasy, G.; Cahen, D.; Cohen, R.; Shanzer, A.; Vilan, A. *Acc. Chem. Res.* **2002**, *35*, 121–128.
(6) Lopinski, G. P.; Wayner, D. D. M.; Wolkow, R. A. *Nature* **2000**, *406*, 48–51.
(7) Zhang, G. *Electrochemistry of Silicon and its Oxide*; Springer-Verlag: Berlin, 2001.
(8) Linford, M. R.; Chidsey, C. E. D. *J. Am. Chem. Soc.* **1993**, *115*, 12631–12632.
(9) Linford, M. R.; Fenter, P.; Eisenberger, P. M.; Chidsey, C. E. D. *J. Am. Chem. Soc.* **1995**, *117*, 3145–3155.
(10) Buriak, J. M. *Chem. Commun.* **1999**, 1051–1060.
(11) Ulman, A. *Chem. Rev.* **1996**, *96*, 1533–1554.
(12) Sagiv, J. *J. Am. Chem. Soc.* **1980**, *102*, 92–98.
(13) Ulman, A. *An Introduction to Ultra-thin Organic Films*; Academic Press: New York, 1991.
(14) Sagiv, J. *Isr. J. Chem.* **1980**, *18*, 346–353.
(15) Sagiv, J. *Isr. J. Chem.* **1980**, *18*, 339–345.
(16) Roth, K. M.; Yasseri, A. A.; Liu, Z.; Dabke, R. B.; Malinovskii, V.; Schweikart, K.-H.; Yu, L.; Tiznado, H.; Zaera, F.; Lindsey, J. S.; Kuhr, W. G.; Bocian, D. F. *J. Am. Chem. Soc* **2003**, *125*, 505–517.
(17) Rohde, R. D.; Agnew, H. D.; Yeo, W.-S.; Bailey, R. C.; Heath, J. R. *J. Am. Chem. Soc.* **2006**, *128*, 9518–9525.
(18) Seitz, O.; Böcking, T.; Salomon, A.; Gooding, J. J.; Cahen, D. *Langmuir* **2006**, *22*, 6915–6922.
(19) Eagling, R. D.; Bateman, J. E.; Goodwin, N. J.; Henderson, W.; Horrocks, B. R. *J. Chem. Soc., Dalton Trans.* **1998**, 1273–1276.
(20) Böcking, T.; Salomon, A.; Cahen, D.; Gooding, J. J. *Langmuir* **2007**, *23*, 3236–3241.
(21) Cerofolini, G. F.; Arena, G.; Camalleri, C. M.; Galati, C.; Reina, S.; Renna, L.; Mascolo, D. *Nanotechnology* **2005**, *16*, 1040–1047.
(22) Puniredd, S. R.; Assad, O.; Haick, H. *J. Am. Chem. Soc.* **2008**, *130*, 9184–9185.
(23) Böcking, T.; James, M.; Coster, H. G. L.; Chilcott, T. C.; Barrow, K. D. *Langmuir* **2004**, *20*, 9227–9235.
(24) Böcking, T.; Kilian, K. A.; Gaus, K.; Gooding, J. J. *Langmuir* **2006**, *22*, 3494–3496.

(25) Cicero, R. L.; Wagner, P.; Lingford, M.; Hawker, C. J.; Waymouth, R. M.; Chidsey, C. E. D. *Polym. Prepr.* **1997**, *38*, 904–905.
(26) Sieval, A. B.; Demirel, A. L.; Nissink, J. W. M.; Linford, M. R.; van der Maas, J. H.; de Jeu, W. H.; Zuilhof, H.; Sudhoelter, E. J. R. *Langmuir* **1998**, *14*, 1759–1768.
(27) Strother, T.; Hamers, R. J.; Smith, L. M. *Nucleic Acids Res.* **2000**, *28*, 3535–3541.
(28) Ciampi, S.; Le Saux, G.; Harper, J. B.; Gooding, J. J. *Electroanalysis* **2008**, *20*, 7.
(29) Ciampi, S.; Böcking, T.; Kilian, K. A.; James, M.; Harper, J. B.; Gooding, J. J. *Langmuir* **2007**, *23*, 9320–9329.
(30) Decker, F.; Cattaruzza, F.; Coluzza, C.; Flamini, A.; Marrani, A. G.; Zanoni, R.; Dalchiele, E. A *J. Phys. Chem. B* **2006**, *110*, 7374–7379.
(31) Webb, L. J.; Michalak, D. J.; Biteen, J. S.; Brunschwig, B. S.; Chan, A. S. Y.; Knapp, D. W.; Meyer, H. M., III; Nemanick, E. J.; Traub, M. C.; Lewis, N. S. *J. Phys. Chem. B* **2006**, *110*, 23450–23459.
(32) Ciampi, S.; Eggers, P. K.; Le Saux, G.; James, M.; Harper, J. B.; Gooding, J. J. *Langmuir* **2009**, *25*, 2530–2539.
(33) Burmeister, F.; Badowsky, W.; Braun, T.; Wieprich, S.; Boneberg, J.; Leiderer, P. *Appl. Surf. Sci.* **1999**, *144*−*145*, 461–466.
(34) Salomon, A.; Böcking, T.; Gooding, J. J.; Cahen, D. *Nano Lett.* **2006**, *6*, 2873–2876.
(35) Lu, M.; Li, X. H.; Yu, B. Z.; Li, H. L. *J. Colloid Interface Sci.* **2002**, *248*, 376–382.
(36) Zhao, J.; Bradbury, C. R.; Huclova, S.; Potapova, I.; Carrara, M.; Fermin, D. J. *J. Phys. Chem. B* **2005**, *109*, 22985–22994.
(37) Zhao, J.; Wasem, M.; Bradbury, C. R.; Fermin, D. J. *J. Phys. Chem. C* **2008**, *112*, 7284–7289.
(38) Hauquier, F.; Pastorin, G.; Hapiot, P.; Prato, M.; Bianco, A.; Fabre, B. *Chem. Commun.* **2006**, 4536–4538.
(39) Yu, J.; Shapter, J. G.; Quinton, J. S.; Johnston, M. R.; Beattie, D. A. *Phys. Chem. Chem. Phys.* **2007**, *9*, 510–520.
(40) Zhao, J.; Bradbury, C. R.; Fermin, D. J. *J. Phys. Chem. C* **2008**, *112*, 6832–6841.
(41) Su, L.; Gao, F.; Mao, L. *Anal Chem* **2006**, *78*, 2651–2657.
(42) Shein, J.; Lai, L. M. H.; Eggers, P. K.; Paddon-Row, M. N.; Gooding, J. J. *Langmuir* **2009**, *25*, 11121–11128.
(43) Liu, J.; Chou, A.; Rahmat, W.; Paddon-Row, M. N.; Gooding, J. J. *Electroanalysis* **2005**, *17*, 38–46.
(44) Horswell, S. L.; O'Neil, I. A.; Schiffrin, D. J. *J. Phys. Chem. B* **2003**, *107*, 4844–4854.
(45) Chou, A.; Eggers, P. K.; Paddon-Row, M. N.; Gooding, J. J. *J. Phys. Chem. C* **2009**, *113*, 3203–3211.
(46) Brust, M.; Bethell, D.; Kiely, C. J.; Schiffrin, D. J. *Langmuir* **1998**, *14*, 5425–5429.
(47) Bradbury, C. R.; Zhao, J.; Fermin, D. J. *J. Phys. Chem. C* **2008**, *112*, 10153–10160.
(48) Bethell, D.; Brust, M.; Schiffrin, D. J.; Kiely, C. *J. Electroanal. Chem.* **1996**, *409*, 137–143.
(49) Turkevich, J.; Stevenson, P. C.; Hillier, J. *Discuss. Faraday Soc.* **1951**, *11*, 55–75.
(50) Bourg, M.-C.; Badia, A.; Lennox, R. B. *J. Phys. Chem. B* **2000**, *104*, 6562–6567.
(51) Uematsu, M.; Kageshima, H.; Shiraishi, K. *Jpn. J. Appl. Phys., Part 2* **2000**, *39*, L1135–L1137.
(52) Ubara, H.; Imura, T.; Hiraki, A. *Solid State Commun.* **1984**, *50*, 673–675.
(53) Burrows, V. A.; Chabal, Y. J.; Higashi, G. S.; Raghavachari, K.; Christman, S. B. *Appl. Phys. Lett.* **1988**, *53*, 998–1000.
(54) Kilian, K. A.; Böcking, T.; Gooding, J. J. *Chem. Commun.* **2009**, 630–640.

AM900427W